IL-17 and immunologically induced senescence regulate response to injury in osteoarthritis

Heather J. Faust,[1] Hong Zhang,[1] Jin Han,[1] Matthew T. Wolf,[1] Ok Hee Jeon,[2] Kaitlyn Sadtler,[1] Alexis N. Peña,[1] Liam Chung,[1] David R. Maestas Jr.,[1] Ada J. Tam,[3] Drew M. Pardoll,[3,4] Judith Campisi,[5] Franck Housseau,[3] Daohong Zhou,[6] Clifton O. Bingham III,[7] and Jennifer H. Elisseeff[1,3]

[1]Translational Tissue Engineering Center, Wilmer Eye Institute and Department of Biomedical Engineering, Johns Hopkins University School of Medicine, Baltimore, Maryland, USA. [2]Department of Biomedical Sciences, Korea University College of Medicine, Seoul, South Korea. [3]Bloomberg-Kimmel Institute for Cancer Immunotherapy and [4]Sidney Kimmel Comprehensive Cancer Center, Johns Hopkins University School of Medicine, Baltimore, Maryland, USA. [5]Buck Institute for Research on Aging, Novato, California, USA. [6]Department of Pharmacodynamics, College of Pharmacy, University of Florida, Gainesville, Florida, USA. [7]Division of Rheumatology, Johns Hopkins University School of Medicine, Baltimore, Maryland, USA.

Senescent cells (SnCs) are implicated in the pathogenesis of age-related diseases including osteoarthritis (OA), in part via expression of a senescence-associated secretory phenotype (SASP) that includes immunologically relevant factors and cytokines. In a model of posttraumatic OA (PTOA), anterior cruciate ligament transection (ACLT) induced a type 17 immune response in the articular compartment and draining inguinal lymph nodes (LNs) that paralleled expression of the senescence marker p16[INK4a] (*Cdkn2a*) and p21 (*Cdkn1a*). Innate lymphoid cells, $\gamma\delta^+$ T cells, and CD4$^+$ T cells contributed to IL-17 expression. Intra-articular injection of IL-17–neutralizing antibody reduced joint degeneration and decreased expression of the senescence marker *Cdkn1a*. Local and systemic senolysis was required to attenuate tissue damage in aged animals and was associated with decreased IL-17 and increased IL-4 expression in the articular joint and draining LNs. In vitro, we found that Th17 cells induced senescence in fibroblasts and that SnCs skewed naive T cells toward Th17 or Th1, depending on the presence of TGF-β. The SASP profile of the inflammation-induced SnCs included altered Wnt signaling, tissue remodeling, and cell-cycle pathways not previously implicated in senescence. These findings provide molecular targets and mechanisms for senescence induction and therapeutic strategies to support tissue healing in an aged environment.

Introduction

Regenerative medicine strategies aim to promote new tissue development but are often limited by systemic and environmental inhibitory factors such as aging or infection. Cellular senescence is associated with aging and age-related chronic diseases such as diabetes, cardiovascular disease, muscle decline, Alzheimer's, and osteoarthritis (OA) (1–4). Though it contributes to aged-related pathologies, cellular senescence also plays beneficial roles during development and wound healing in the regulation of tissue repair and remodeling (5). Senescent cells (SnCs) are characterized by permanent growth arrest combined with active secretion of soluble factors that comprise the senescence-associated phenotype (SASP). The SASP is implicated in SnC-associated pathogenesis and regulatory roles in tissue development and repair (6). It includes numerous cytokines that are known to regulate immune cells, suggesting that SnCs may exert and amplify their effects through modulation of the immune system, and, in turn, these immune responses may impact SnCs and modify the SASP (7).

Cartilage is historically considered a tissue that cannot repair when damaged. Articular joint injury induces the development of SnCs that accumulate rather than being cleared as they are during the normal healing process in other tissues such as skin (5). Senescence induction after joint injury leads to chronic inflammation, tissue degeneration, and eventually OA in animal models (1). Clearance of SnCs in the joint using transgenic models or senolytic drugs attenuates OA development in young animals. In aged animals, clearance of SnCs in the joint reduces pain symptoms, but it is unclear whether the tissue structure can be rescued (1, 8). Aging
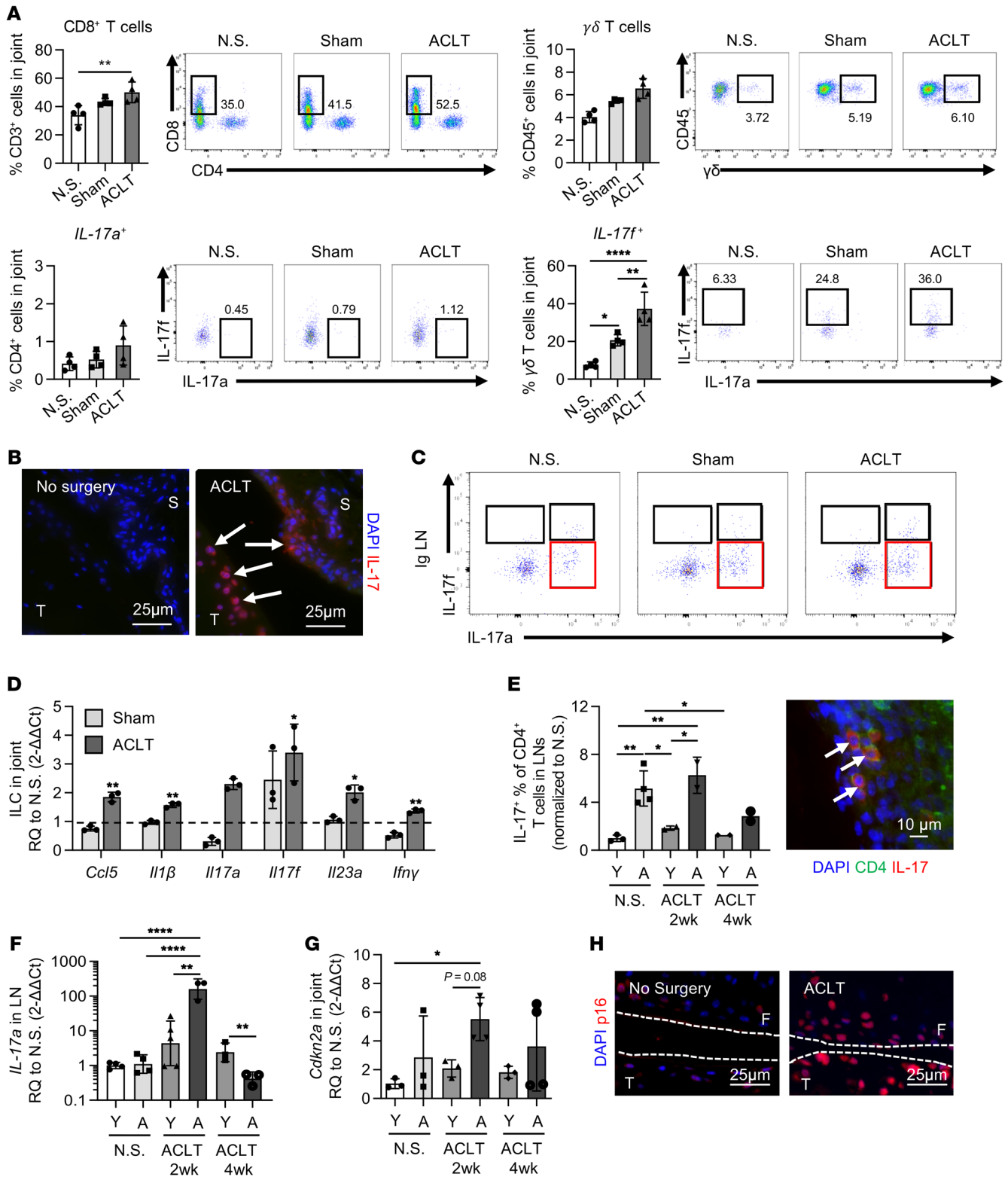
Figure 1. Adaptive immune cells respond to traumatic joint injury with a type 17 immune response. (**A**) Multiparametric flow cytometric analysis of CD8$^+$, CD4$^+$, and γδ$^+$ T cells (CD45$^+$CD3$^+$) isolated from the joint compartment 1 week after sham surgery and ACLT compared with control mice with no surgery (N.S.) (n = 4). (**B**) Immunofluorescence of IL-17 in the synovium and cartilage 1 week after ACLT compared with no surgery in young mice. Scale bars: 25 μm. (**C**) Flow cytometric data showing IL-17a and IL-17f expression in ILCs from inguinal (Ig) LNs 4 weeks after ACLT (CD3$^-$Thy1.2$^+$NK1.1$^-$). (**D**) Quantification of mRNA expression for inflammatory markers in ILCs (CD3$^-$Thy1.2$^+$) sorted from the joint compartment 2 weeks after ACLT (n = 2). (**E**) Percentage of Th17 cells in young (Y) and 18-month-old aged (A) animals 2 and 4 weeks after ACLT in the inguinal LNs, as determined by flow cytometry and immunofluorescence staining for CD4 and IL-17 in LNs from young mice 2 weeks after ACLT. Scale bar: 10 μm. (**F**) Quantification of *Il17* mRNA expression in LN tissue (n = 3). (**G**) Quantification of *Cdkn2a* mRNA expression in young and aged animal joints with no surgery and in joints 2 and 4 weeks after ACLT (n = 3). (**H**) p16 staining of ACLT cartilage and no-surgery cartilage from young mice. Scale bars: 25 μm. Data indicate the mean ± SD. *P < 0.05, **P < 0.01, and ****P < 0.001, by 1-way ANOVA with Holm-Šidák multiple-comparisons test. All groups were compared with each other. (**E–G**) Separate 1-way ANOVAs were performed for each time point. F, femur; S, synovium; T, tibia; RQ, relative quantification.

is associated with numerous physiological changes including a decline of the immune system, which regulates tissue repair and may also be responding to SnCs (9, 10). The number of immune cells decreases with aging, but inflammation in the body broadly increases (11, 12). "Inflammaging" is characterized in part by altered T cell populations including increased ratios of Th17 cells compared with Tregs in peripheral blood (13, 14).

The immune profile of posttraumatic OA (PTOA) and its potential connection to SnCs that develop after injury or accumulate with aging is unknown (15). OA has historically been considered primarily a localized disease, characterized by tissue loss from mechanical "wear and tear." Anecdotal observations of Th17 cells in the blood of patients with OA suggest an immunological component of disease, but low numbers of immune cells in cartilage and few observed T cells in the synovium of patients with OA have thus far precluded a correlation (16–18). In preclinical models, molecular mechanisms of a T cell response to joint injury remain unexplored. Although unknown in OA, other inflammation-mediated joint conditions including rheumatoid and psoriatic arthritis (PsA), and spondyloarthritis (SpA), are classified as systemic autoimmune diseases and are associated with Th17 immune signatures (19). Current therapies for PsA and SpA include systemically delivered IL-17 inhibitors that successfully reduce disease symptoms and decrease the progression of joint damage (20). Clinical perspectives of OA today suggest that it is also a systemic disease with broad physiological impact, but it is unclear how local injury produces systemic sequelae (21). Although there is evidence to suggest local inflammation in OA synovium, approaches targeting the proinflammatory cytokines IL-1 and TNF have not been successful, and targeting IL-17 has not been tested (22, 23). The senescence-associated immune ("sen-immune") profile provides a potential mechanistic link between the immune response to injury, aging, and senescence.

Here, we explore the connection between SnCs and the immune system in young and aged animals with OA. We performed in-depth immune profiling after posttraumatic injury in the

articular joint and identified a Th17 immune signature in the joint and draining lymph nodes (LNs). The expression of *Il17* increased in parallel with markers of SnCs and decreased after senolysis. In vitro coculture studies further validated the Th17-SnC feedback, with Th17 cells inducing senescence in healthy fibroblasts and senescent fibroblasts inducing Th17 skewing in naive T cells. Further expression profiling of the immunologically induced SnCs revealed a unique SASP characterized by altered Wnt signaling, tissue stemness (24), metabolic pathways not previously implicated in senescence, and genes that regulate STAT3 and impact Th17 differentiation. SnC clearance reduced Th17 cells and tissue *Il17* gene expression and decreased tissue damage in young animals. In aged animals, IL-17 decreased with local SnC clearance but did not reduce tissue damage. We found that cartilage structure could be rescued in the articular joint of aged animals with combined local and systemic senolysis that resulted in increased *Il4* expression in the joint and draining LNs. We found that senolytic efficacy in reducing IL-17 and decreasing tissue damage was lost in the *Il4r$^{-/-}$* mouse. Tissue integrity and *Il4* expression in the articular joint was rescued in the nonhealing articular wound and in aged organisms by removing senescence and immune-related inhibitory factors. These findings provide insight into the interactions between SnCs and the immune system and strategies to promote tissue healing in age-related OA.

Results

Articular joint injury induces IL-17 expression in innate lymphoid cells, γδ T cells, and CD4$^+$ T cells. We performed flow cytometry on a single-cell suspension from joint tissue after anterior cruciate ligament transection (ACLT) in a murine OA model to define the adaptive immune response to trauma in the articular joint and correlate it with the development of SnCs (Figure 1A). The ACLT model induces SnC development and cartilage degeneration that mimic characteristics of PTOA, including cartilage degeneration and joint pain. As a control for ACL transection, mice underwent sham surgery, in which the joint capsule was opened but the ACL was not transected. One week after ACLT, the percentage of CD8$^+$ T cells increased from 34% to 50% in the articular joint compartment (cartilage, subchondral bone, and synovium) compared with the no-surgery controls, and γδ$^+$ T cells increased from 4% to 6.5% (Figure 1A). The CD4$^+$ T cells increased IL-17a protein expression from 0.4% to 0.9%, and γδ T cells significantly increased IL-17f protein expression from 7.5% to 37% after ACLT (Figure 1A). The sham-operated joints had intermediate levels of these cell populations: 43.3% CD8$^+$ T cells, 5.46% γδ$^+$ T cells, 0.52% IL-17a$^+$CD4$^+$ T cells, and 20.6% IL-17f$^+$ γδ T cells. IFN-γ and IL-4 did not significantly change after sham or ACLT injury relative to the no-surgery controls (Supplemental Figure 1, A–D; supplemental material available online with this article; https://doi.org/10.1172/JCI134091DS1). The number of IL-4$^+$CD4$^+$ T cells in the joint was small, precluding further analysis (Supplemental Figure 1D). Absolute T cell numbers in the joint space did not change by 2 or 4 weeks after surgery (Supplemental Figure 1, E and F).

Immunofluorescence staining confirmed the presence of IL-17 and its localized expression on the cartilage surface and synovial tissue (Figure 1B). Human synovium from patients diagnosed with OA contained cells expressing IL-17, whereas no expression of IL-17 was
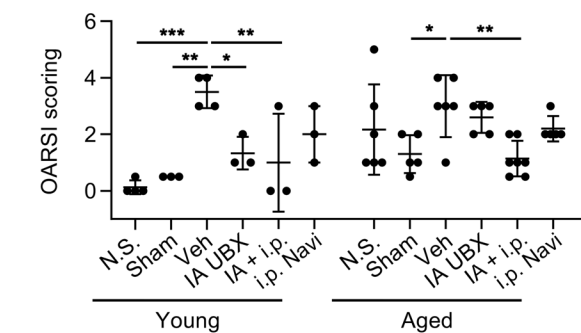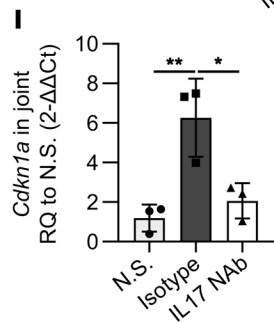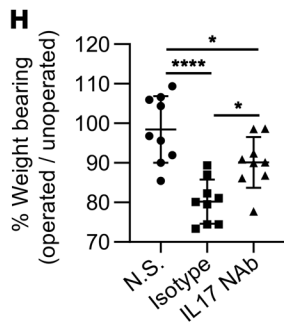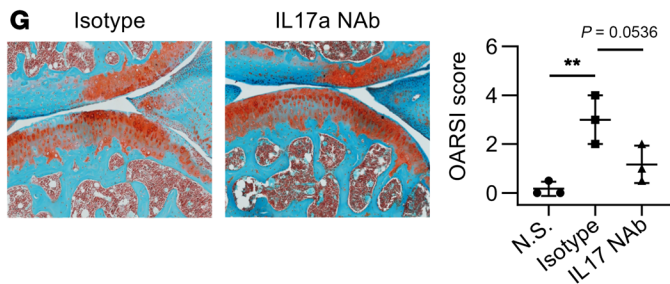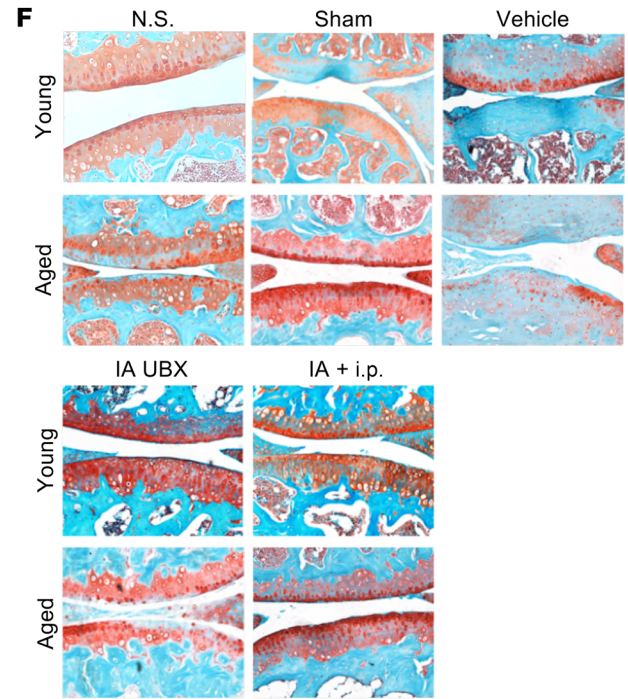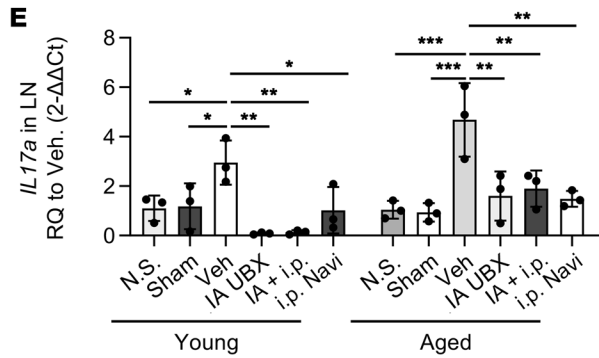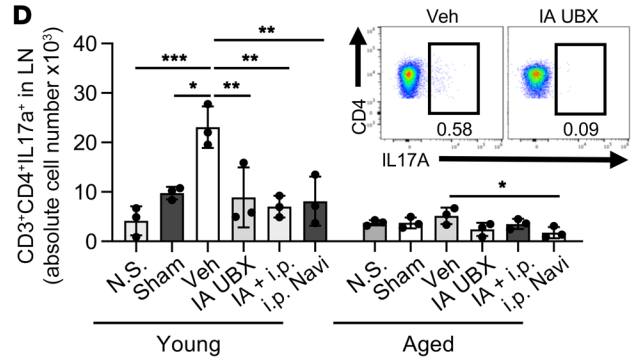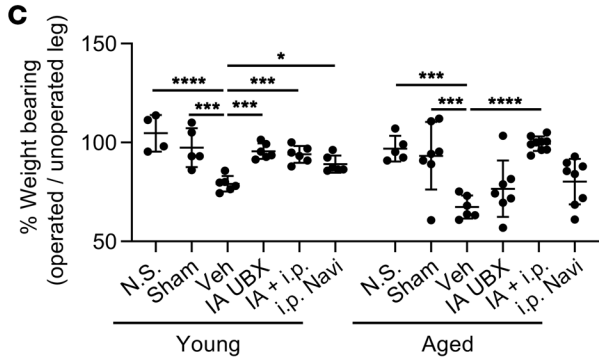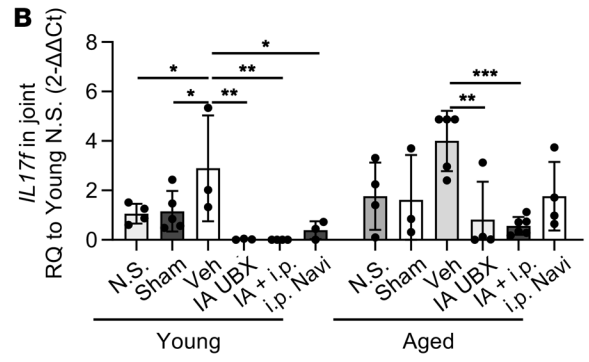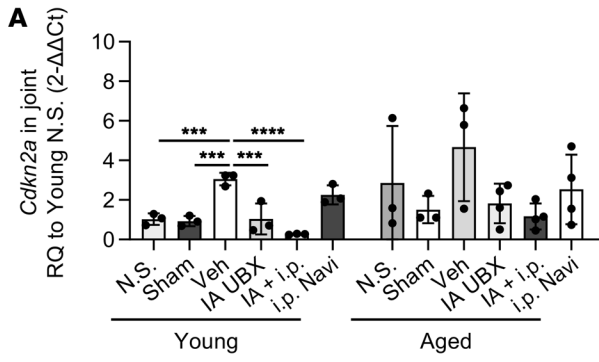
Figure 2. Clearance of SnCs reduces the IL-17 immune signature. (**A**) Quantification of *Cdkn2a* mRNA expression in articular joints of young and aged mice that had no surgery (N.S.), mice that underwent sham surgery, and mice that underwent ACLT and treatment with vehicle (Veh), i.a. UBX0101 (UBX), i.a. UBX plus i.p. Navi, or i.p. Navi (*n* = 3–6). (**B**) Quantification of *Il17f* mRNA expression in articular joints of young and aged mice as in **A** (*n* = 3–6). (**C**) Percentage of weight placed on the operated limb versus the contralateral control limb by in mice as in **A** (*n* = 3–6). (**D**) Quantification of CD4⁺IL-17a⁺ cells from inguinal LNs of mice and representative flow plots (*n* = 3 for each group). (**E**) Quantification of mRNA expression for *Il17a* in inguinal LN tissue (*n* = 3 for each group). (**F**) Representative safranin-O images of joints and OARSI scores for mice as in **A** (*n* = 3–6). Original magnification, ×20. (**G**) Representative safranin-O images of joints and OARSI scores after ACLT and treatment with isotype or IL-17a NAb (*n* = 3). Original magnification, ×20. (**H**) Percentage of weight placed on the operated limb versus the contralateral control limb for mice that had no surgery or mice after ACLT that were treated with either the isotype control or a IL-17a NAb (*n* = 9). (**I**) Quantification of *Cdkn1a* mRNA expression in articular joints (*n* = 3). Data indicate the mean ± SD. *$P < 0.05$, **$P < 0.01$, ***$P < 0.005$, and ****$P < 0.001$, by 1-way ANOVA with Holm-Šidák multiple-comparisons test. All groups were compared with each other. (**A**–**F**) Separate 1-way ANOVAs were performed for young and aged groups, and experimental groups were compared with the control group (vehicle-treated mice).

detectable in tissue from donors without diagnosed OA (Supplemental Figure 2A). We found that IL-23, a cytokine associated with stabilization of the Th17 subset and pathological fibrosis, was also present in OA synovium (Supplemental Figure 2A and ref. 25). Vascular channels directly connecting the bone marrow to the joint space were visible near ligament insertion sites, providing access to cell infiltrate after ACLT including F4/80⁺CD11b⁺ immune cells (Supplemental Figure 3). Similar channels and access to the bone marrow develop in inflammatory arthritis but are also found in normal tissue (26).

Innate lymphocytes (ILCs) are tissue-resident immune cells of lymphoid lineage that can rapidly respond to stimuli in a nonspecific manner, with effector profiles similar to those of T cells (27, 28). ACLT injury increased IL-17a⁺ ILC numbers in the draining LNs 4 weeks after surgery (Figure 1C). ILCs (CD45⁺CD3⁻Thy1.2⁺) sorted from the articular joint 2 weeks after ACLT expressed significantly higher levels of cytokine genes related to a type 17 immune response, including *Il17f* and *Il23a*, as well as the inflammatory gene *Infg* and the T cell chemokine *Ccl5*, characteristic of ILC groups 1 and 3, respectively (Figure 1D, Supplemental Figure 2B, and ref. 29). Sham surgery also induced the upregulation of several inflammatory genes in ILCs, but not *Il17f* and *Il23a*.

Engagement of the adaptive immune system after injury and OA development introduces the potential for a systemic effect and observable changes in lymphatics including the inguinal LN that drains lymph from the articular joint. *Il17a and Il17f* gene expression significantly increased in inguinal LNs 4 weeks after ACLT but not after sham surgery (Supplemental Figure 2C). Injury severity also altered the kinetics of the immune response and senescence development within the joint. Sham surgery led to mild but visible cartilage degeneration after 4 weeks as well as lower levels of pain (Figure 2C and Supplemental Figure 2D). After sham surgery, *Cdkn2a* expression in the joint increased by 1 week and then steadily decreased over 4 weeks, and *Cdkn1a* similarly increased by 1 week, peaked at 2 weeks, and decreased significantly by week 4 (Supplemental Figure 2E). In contrast, after ACLT injury, *Cdkn2a* and *Cdkn1a* expression moderately increased at later time points after injury and remained upregulated, suggestive of a low level of chronic inflammation (Supplemental Figure 2E). Sham surgery also resulted in the upregulation of inflammatory genes, but this generally peaked 1 and 2 weeks after surgery and was mostly resolved by week 4. Expression of the immunosuppressive cytokine *Il10* also increased in sham-operated joints 1 week after surgery (Supplemental Figure 2B). The increase in *Il10* after sham surgery was followed by downregulation of *Il10*, *Il17f*, *Csf2*, and *Cdkn2a* expression to preinjury levels by week 4 after injury. Unlike the sham-operated joints, *Il10* expression levels did not change after ACLT, and expression of *Cdkn2a* remained upregulated out to week 4. Normal healing involves an initial proinflammatory phase and the presence of SnCs (5, 30). The gene expression changes in the sham-operated group indicated an initial proinflammatory state (including increased *Csf2*, *Il17f*, and *Il23a* expression) with increased senescence burden, which is probably beneficial for healing and resolves over time. However, the ACLT group did not have this initial burst of beneficial acute inflammation or senescence and had a lower level of these cytokines that persist over time. This chronic inflammation and SnC accumulation likely contributes to disease pathology. These findings suggest that the composition and kinetics of the immune response and the number and location of SnCs may determine healing outcomes and progression to chronic disease.

The type 17 immune response to articular injury increases with age. Aging is associated with an increasing burden of SnCs throughout the body that may be exacerbated with injury (31). In young animals, SnCs develop on the articular surface after ACLT injury. Older animals have higher levels of *Cdkn2a* expression within joints before injury and a greater number of SnCs throughout the articular cartilage after injury compared with young animals. Markers of senescence increase even further after ACLT and development of PTOA in aged animals (1). Previous studies that investigated the removal of SnCs in the articular joint of older animals after injury found reduced tissue degeneration and pain, but there was minimal new tissue development (1).

Aging is also associated with changes in the immune system that may influence the observed type 17 response to ACLT surgery that we profiled in young animals. To determine whether injury in the aged animals (18 months or older) produced greater levels of inflammation in addition to senescence, we performed flow cytometry on cells from the draining LNs. We found that the percentage of IL-17⁺CD4⁺ T cells in the LNs of aged animals before surgical intervention was 5 times higher than in the young animals (Figure 1E). Immunohistochemical analysis also identified IL-17⁺CD4⁺ T cells in the draining LNs after ACLT (Figure 1E). Increasing expression of *Cdkn2a* in the joint compartment paralleled the increases in IL-17a found in the draining LNs (Figure 1, F and G). We also detected increased expression of p16 at the protein level in the cartilage of mice after ACLT (Figure 1H). The number of CD4⁺ T cells in the draining LNs of healthy and ACLT aged animals was significantly lower compared with that in the younger animals (Supplemental Figure 4). However, expression of *Il17a* in the aged LNs was significantly higher after injury, similar to what we observed in the young animals, suggesting that higher levels of *Il17* were expressed per cell or that there were other cell sources (Figure 1F).
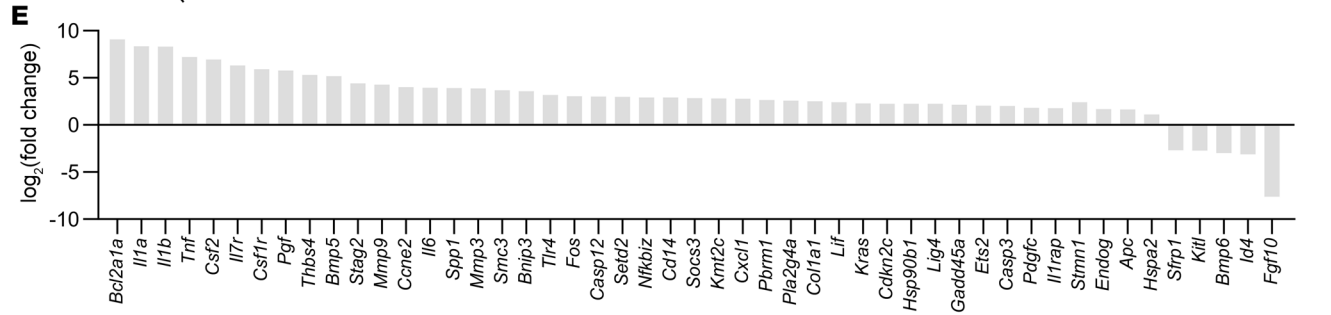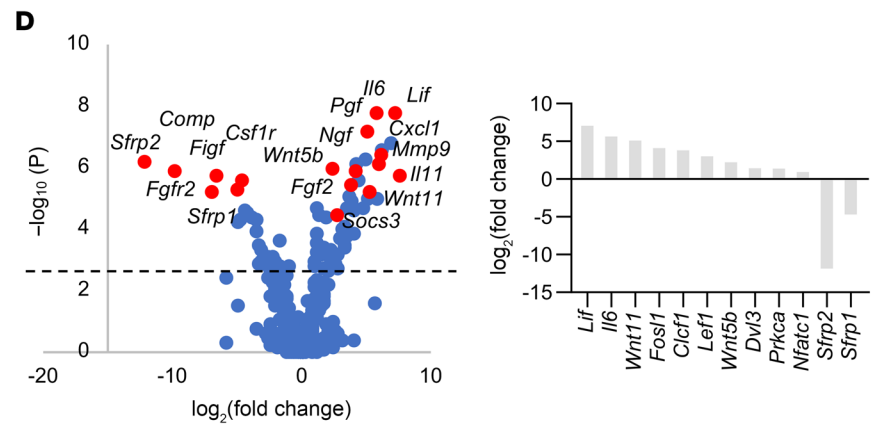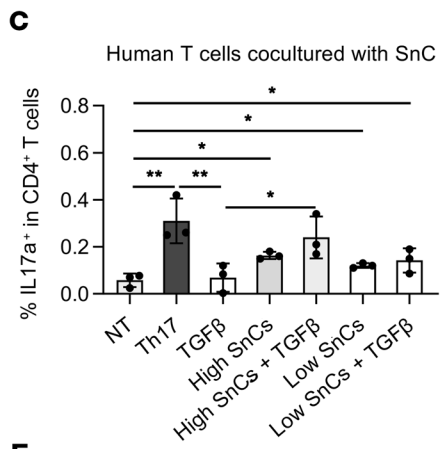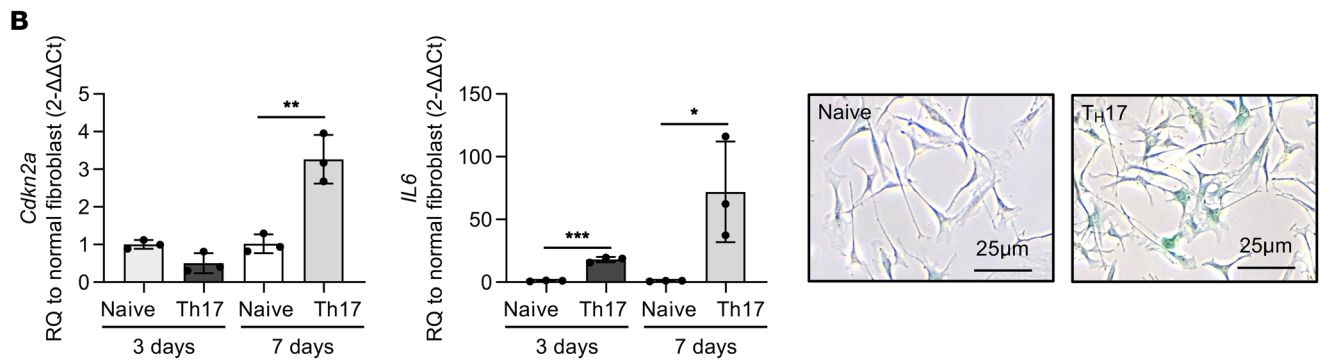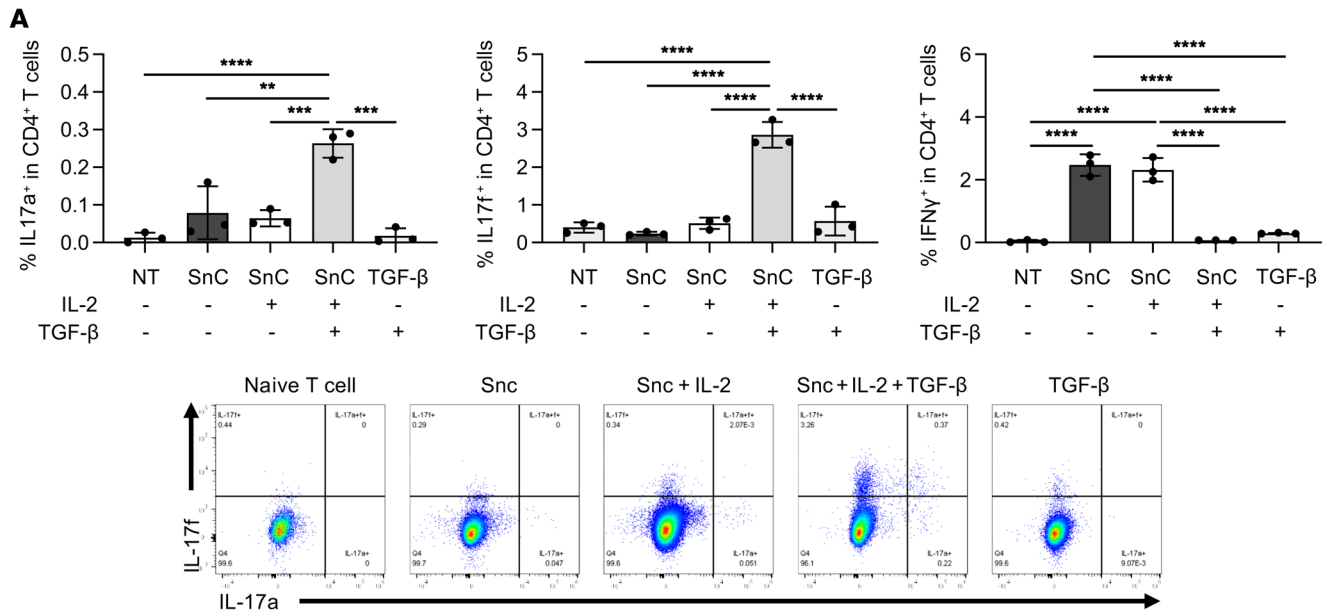
Figure 3. Inflammation-induced senescence in fibroblasts cultured with Th17 cells and T cell skewing by senescent fibroblasts. (**A**) Percentage of mouse CD4$^+$IL-17a$^+$, CD4$^+$IL-17f$^+$, and CD4$^+$IFN-γ$^+$ T cells in coculture conditions: naive T cells alone (NT), SnC coculture, SnCs plus IL-2 plus TGF-β coculture, media with TGF-β (n = 3 for each group). Representative flow plots are shown. (**B**) Quantification of *Cdkn2a* and *Il6* mRNA expression in fibroblasts cocultured with naive CD4$^+$ T cells and Th17 cells (n = 3 for each group). Representative images of SA–β-gal staining of fibroblasts cocultured with naive CD4$^+$ T cells and Th17 cells are shown. Scale bars: 25 μm. (**C**) Percentage of human CD4$^+$IL-17a$^+$ T cells after 7 days in coculture. Conditions from left to right: no coculture (NT), Th17 positive control, high percentage of SnCs coculture, high percentage of SnCs plus IL-2 plus TGF-β coculture, low percentage of SnCs coculture, low percentage of SnCs plus IL-2 plus TGF-β coculture (n = 3 for each group). (**D**) Volcano plot of Th17 cocultured cells normalized to normal fibroblasts. The dotted line denotes P = 0.05. Graph on the right indicates differentially regulated genes related to STAT3 and Wnt signaling. (**E**) Differential expression of the top-50 genes in immune-induced senescence (Th17 coculture) compared with irradiation-induced senescence, 7 days after senescence induction (n = 3). Data indicate the mean ± SD. *P < 0.05 and **P < 0.01, by 1-way ANOVA with Holm-Šidák multiple-comparisons test. All groups were compared with each other. A 2-tailed Student's t test was performed within each time point in **B**.

The increased senescence burden in the older animals correlated with increased IL-17 expression in the draining LNs before and after injury (Figure 1, E–H). The increase in joint senescence burden was more pronounced in animals that had multiple intra-articular (i.a.) injections compared with only an initial ACLT (Figure 1G vs. Figure 2A). Aged animals experienced significantly more pain after injury compared with the younger animals (Figure 2C). Histologically, the aged joints had more variable tissue quality before injury that further deteriorated after injury, resulting in thinner cartilage and reduced proteoglycan staining (Figure 2F). The reduced tissue quality in the aged animals and increased heterogeneity before injury were reflected in their Osteoarthritis Research Society International (OARSI) scores (Figure 2F).

Clearance of SnCs reduces type 17 immune signatures in young and aged mice with PTOA. Since the increases in IL-17 paralleled the increase in senescence (Figure 1, E–G), we next sought to determine whether SnC clearance affects the immune landscape in the articular joint and draining LNs. i.a. injection of the senolytic UBX0101, an inhibitor of MDM2-p53 protein interaction, decreased *Cdkn2a* expression in young and aged mice after ACLT (1). Since i.a. injection of UBX0101 was not adequate to restore the aged joint structure in previous studies, we investigated multiple senolytic drug regimens designed to improve the response in aged animals. Navitoclax (Navi) is a senolytic agent that was previously demonstrated to reduce senescence burden in multiple tissues in aged animals (without injury). We therefore evaluated a combination of i.a. UBX0101 and systemic Navi delivered i.p. i.a. injection of UBX0101 and combined i.a. UBX0101 with i.p. Navi significantly reduced *Cdkn2a* expression in young animals compared with vehicle alone, with combined treatment achieving the greatest reduction (Figure 2A). Combined i.a. UBX0101 and i.p. Navi achieved the greatest reduction in *Cdkn2a* expression among the senolytic regimens, although it was not statistically significant because of the increased variability in the aged animals (Figure 2A).

To determine whether there was a correlation between SnC clearance and the immune profile, we evaluated the cellular and molecular changes in the joint and draining LNs 4 weeks after surgery. We found that *Il17f* expression in the joint significantly decreased after clearance of SnCs (Figure 2B). Similarly, the number of Th17 cells and *Il17a* expression in the draining LNs significantly decreased after senolytic treatment (Figure 2, D and E). The decrease in *Cdkn2a* expression and type 17 immune response signatures correlated with improved joint structure and function, although the response varied with age (Figure 2F and Supplemental Figure 5A). In young animals, weight bearing on the operated limb significantly improved after senolysis compared with vehicle control treatment and was statistically similar to that observed in the sham-operated and no-surgery control animals (Figure 2C). OARSI scores for young animals significantly improved after i.a. and i.a. plus i.p. senolytic treatment compared with vehicle injections, and this was accompanied by improved proteoglycan staining (Figure 2F). In aged animals, i.a. senolytic treatment mildly improved the pain response (Figure 2C), but we observed minimal improvement in joint structure, indicating a failure to reduce tissue damage in response to ACLT injury (Figure 2F).

To further probe the connection between senescence and Th17, we evaluated the expression of SASP factors that are relevant to Th17 skewing of T cells. IL-6, IL-1β, and TGF-β are cytokines known to stimulate Th17 development. *Il6* expression substantially increased in the joint after ACLT in young animals. Aged animals had higher, albeit variable, *Il6* expression compared with young animals before injury and increased *Il6* expression after ACLT. Injection (i.a.) of UBX0101 and combined i.a. UBX0101 plus i.p. Navi significantly reduced *Il6* expression in young animals compared with treatment with vehicle alone, similar to the *Cdkn2a* expression changes (Supplemental Figure 6). While all senolytic regimens reduced *Il6* expression in aged animals after injury, combined i.a. UBX0101 plus i.p. Navi achieved the greatest reduction, although it was not statistically significant, given the increased variability in the aged animals (Supplemental Figure 6). We previously demonstrated that IL-1β expression increased in the joint after injury and decreased after senolytic treatment (1). TGF-β is also found in the joint, and its production is associated with OA development (32). A summary of the proposed senescence-Th17 connection that may be occurring in vivo is outlined in the schematic in Supplemental Figure 13F.

To determine whether Navi treatment directly affects CD4$^+$ T cells, we treated aged animals with senolytics (without any surgical intervention). CD4$^+$ T cell numbers in peripheral blood remained unchanged over 5 weeks in both young and aged animals treated with systemic Navi (Supplemental Figure 7A). CD8$^+$ T cell numbers showed a decreasing trend in both young and aged animals after Navi treatment (P = 0.2933 for young animals, P = 0.0934 for aged animals) (Supplemental Figure 7A). Similarly, Navi treatment did not affect the number of CD4$^+$ T cells in the LNs of aged mice (Supplemental Figure 7B). Although we observed a significant decrease in the number of CD45$^+$ T cells in aged animals compared with young animals, treatment with Navi did not change CD45$^+$ or CD4$^+$ T cell numbers 2 weeks after treatment. With injury and senolytic treatment, the CD4$^+$/CD8$^+$ T cell ratio in the blood increased, whereas the percentage of Th17 cells decreased (Supplemental Figure 8, A–C). Total CD4$^+$ T cell num-
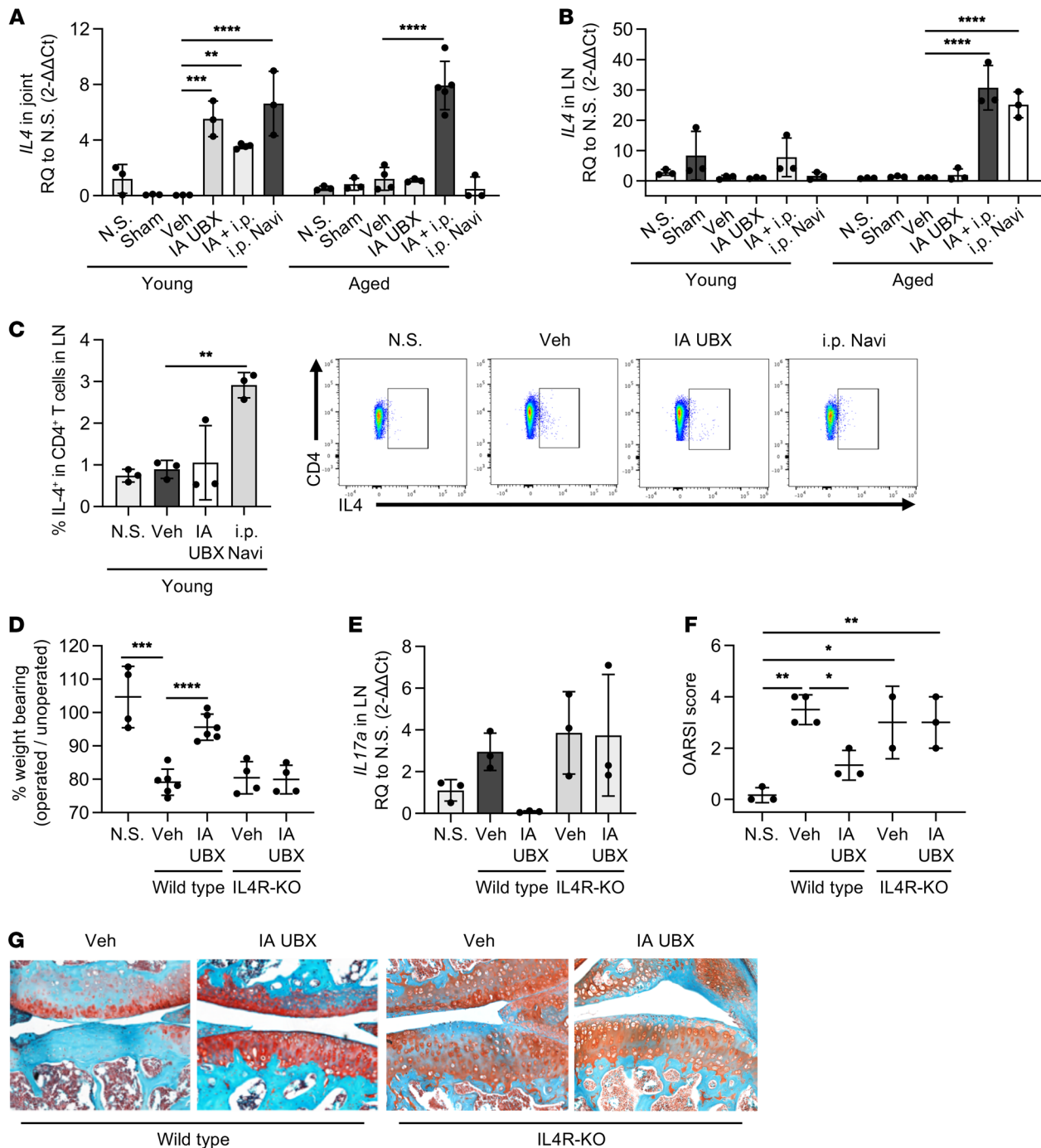
Figure 4. IL-4 is required for wound healing after SnC clearance and IL-17 reduction. (**A**) Quantification of *Il4* mRNA expression in articular joints of young and aged mice (no surgery, sham surgery, after ACLT treated with vehicle, i.a. UBX, i.a. UBX plus i.p. Navi, and i.p. Navi). *n* = 3–5. (**B**) Quantification of *Il4* mRNA expression in inguinal LNs (*n* = 3). (**C**) Percentage of CD4⁺IL-4⁺ T cells in inguinal LNs (*n* = 3). Representative flow plots of cells from LNs from young animals (no surgery, vehicle-treated, i.a. UBX–treated, and i.p. Navi–treated). (**D**) Percentage of weight placed on the operated limb versus the contralateral control limb (*n* = 4). (**E**) Gene expression of *Il17a* in inguinal LNs from WT versus *Il4r⁻/⁻* mice after treatment with senolytic drug (*n* = 3). (**F**) OARSI score of young WT and *Il4r⁻/⁻* joints treated with vehicle or senolytic drug. (**G**) Representative images of young WT or *Il4r⁻/⁻* joints treated with vehicle or senolytic drug. WT vehicle and i.a. UBX images are also shown in Figure 2F. Original magnification, ×20. Data indicate the mean ± SD. *$P < 0.05$, **$P < 0.01$, ***$P < 0.005$, and ****$P < 0.001$, by 1-way ANOVA with Holm-Šidák multiple-comparisons test. Experimental groups were compared with the control group (vehicle).

bers in the draining LNs did not change with senolytic treatment, but the number of Th17 cells decreased, suggesting there was not a direct killing of T cells but a reduction in Th17 development with senolytic treatment (Supplemental Figure 8D).

Since IL-17 paralleled senescence markers and correlated with OA disease progression, we evaluated the effect of i.a. IL-17a inhibition on OA development. An IL-17a neutralizing antibody (NAb) or an isotype control was administered (5 μg/dose, i.a.) every other

day for a total of 5 doses, starting 1 week after surgery. Injection (i.a.) of IL-17a NAb decreased *Cdkn1a* and *Mmp13* expression, whereas it increased expression of *Il4* (Figure 2I and Supplemental Figure 9). However, *Cdkn2a* expression levels did not change. Tissue structure significantly improved with i.a. delivery of IL-17a NAb compared with isotype control treatment (Figure 2G). Further, IL-17a NAb decreased pain compared with isotype control treatment, increasing weight bearing on the operated limb by 10% (Figure 2H). These results suggest that SnC burden and the pathological impact of joint injury are reduced when IL-17a is inhibited.

Aged animals require systemic senolysis to attenuate OA development. It is generally accepted that aging reduces repair capacity, and in the case of the articular joint, the incidence of arthritis and tissue degeneration increases with age. We hypothesized that the reduced capacity of aged animals to achieve tissue repair after local senolysis may be due to systemic factors that are inhibiting tissue repair that could be rescued with systemic clearance of SnCs. Previous research demonstrated that systemic senolytic treatment with Navi reconstituted bone marrow components including hematopoietic precursors and mesenchymal progenitors in aged animals that may be relevant for tissue repair in the joint (33). Moreover, systemic inflammation present in aging may also inhibit tissue repair.

Although we found that IL-17 signatures decreased with all senolytic treatment regimens, only the combined i.a. plus i.p. senolytic treatment resulted in both functional changes in pain and improved tissue structure in aged animals (Figure 2, C and F). Weight-bearing measurements of pain returned to no-surgery levels, and safranin-O staining also revealed consistent improvement in tissue structure with i.a. plus i.p. treatment, as evidenced by thicker cartilage with a smooth, intact surface and strong proteoglycan staining (Figure 2F). Combined i.a. plus i.p. senolytic treatment was the only regimen that significantly improved OARSI scores in aged animals. OARSI scores returned to sham surgery levels, with some animals achieving better scores than aged animals that did not undergo surgical intervention. Injection (i.a.) of both UBX0101 and Navi did not improve the tissue structure, suggesting that systemic senolysis was required to restore tissue-healing capacity in the aged animals (Supplemental Figure 10, A–C).

In young mice, osteophytes significantly decreased after any senolytic treatment (Supplemental Figure 11). In aged mice, only combined i.a. plus i.p. senolytic treatment significantly reduced osteophyte formation, providing further evidence of improvements in tissue structure and disease in the aging animals (Supplemental Figure 11). Both young and aged mice already had cartilage damage 2 weeks after ACLT surgery. The OARSI scores showed improved tissue structure after senolytic treatment, suggesting that the therapy prevents the development of further posttraumatic tissue damage and may potentially induce tissue repair (Supplemental Figure 12).

Positive reinforcement of senescent and Th17 cell differentiation in culture. Senescence and IL-17 production increased and decreased in parallel in vivo, so we tested the interactions and possible mechanistic connections between SnCs and the immune system using in vitro coculture systems (Supplemental Figure 13A). We induced senescence in murine fibroblasts with ionizing radiation and confirmed induction using senescence-associated β-gal (SA–β-gal)

staining (34). Naive T cells activated with IL-2 and cocultured with SnCs increased IFN-γ protein expression levels characteristic of Th1 cells by 62-fold, whereas IL-17 levels did not change (Figure 3A and Supplemental Figure 13B). Addition of TGF-β, a cytokine present in the healthy joint space and upregulated in pathology (32), increased protein expression of both Il-17a and Il-17f by 26-fold and 7-fold, respectively, whereas IFN-γ protein expression decreased. These results suggest that senescent fibroblasts promoted Th17 skewing in the presence of TGF-β, and Th1 skewing without TGF-β (Figure 3A and Supplemental Figure 13F). IL-6 and IL-1β, known SASP factors, and TGF-β are recognized as cytokines that promote T cell differentiation and Th17 skewing (35). We validated the murine coculture results using human OA chondrocytes cultured with CD4+ T cells (Supplemental Figure 13, C and D). The senescent human OA chondrocytes induced Th17 skewing of naive T cells after 7 days of coculture, with TGF-β further promoting the Th17 phenotype (Figure 3C).

Since SnCs and their associated SASP factors can induce Th17 differentiation, we evaluated the impact of Th17 cells on fibroblasts in a coculture model (Supplemental Figure 13E). Expression of the SASP factor *Il6* increased 20- and 60-fold in fibroblasts cocultured with Th17 cells for 3 and 7 days, respectively, compared with coculture with naive T cells (Figure 3B). After 7 days of coculture, *Cdkn2a* expression significantly increased by more than 3-fold, and fibroblasts stained positive for SA–β-gal, further confirming senescence (Figure 3B). These results suggest that Th17 T cells alone can induce senescence in fibroblasts, just as senescent fibroblasts are capable of inducing Th17 skewing, resulting in positive reinforcement of the Th17-Snc sen-immune profile. In other words, a chronic Th17 immune response can induce senescence, which in turn further promotes and reinforces the Th17 phenotype.

Inflammation-induced SnCs express a unique SASP. Further profiling of the inflammation-induced SnCs (Ii-SnCs) using the NanoString platform defined an expression profile that shared some characteristics of the recognized SASP in proliferative, oncogenic, and oxidative damage–induced senescence but also included genes not identified in irradiation-induced SnCs (IR-SnCs), suggesting that Ii-SnCs have a unique SASP. Wnt, STAT3, extracellular matrix, and cell death–associated genes were differentially regulated between the Ii-SnCs and IR-SnCs. Ii-SnCs upregulated STAT3-related genes (*Lif*, *Il6*, *Clcf1*), Wnt signaling genes (*Prkca*, *Dvl3*, *Wnt5b*, *Lef1*, *Wnt11*, *Fosl1*, *Nfatc1*), and extracellular matrix genes (*Mmp9*, *Tnc*, *Hspb1*, *Mmp3*), as well as cell-cycle, apoptosis, and proliferation regulatory genes compared with normal fibroblasts (Figure 3D, Supplemental Figure 14A, and Supplemental Table 1). IR-SnCs increased the expression of cell-cycle, apoptosis, and proliferation regulatory genes and decreased the expression of extracellular matrix genes (*Col3a1*, *Col1a2*, *Col1a1*, *Col11a1*, *Thbs4*) (Supplemental Figure 14B and Supplemental Table 2). Ii-SnCs increased expression of the prototypic SASP factors *Il6*, *Il1b*, and *Tnf* by 4-, 8-, and 7-fold, respectively, relative to IR-SnCs (Figure 3E). Altered expression of cell-cycle genes is a signature of SnCs as they are in growth arrest, but Ii-SnCs significantly increased the expression of *Ccne2*, *Cdkn2c*, *Gadd45a*, *Stag2*, *Smc3*, *Casp12*, and *Casp3*, which did not change in IR-SnCs (Figure 3E). Ii-SnCs increased expression of the IL-17 receptor (*Il17r*), further supporting the type 17 response connection to senescence.

Ii-SnCs expressed unique signatures associated with tissue development, remodeling, and inflammation. Differential expression analysis and gene ontology (GO) supported altered Wnt signaling, upregulation of *Prkca*, *Dvl3*, *Wnt5b*, *Lef1*, *Wnt11*, *Fosl1*, and *Nfatc1*, and downregulation of *Sfrp2* and *Sfrp1* genes, which modulate Wnt signaling. Wnt signaling regulates stem cell survival, promotes stemness, and plays a critical role in embryological development and development of tissue, including cartilage (36). Wnt signaling also converges with STAT3 and leukemia inhibitor factor (*LIF*), another gene significantly upregulated by and unique to the Ii-SnCs. LIF activates STAT3 and is central to both signaling in stem cells and to the development and regulation of T cell fates (37, 38). STAT3 is required for Th17 differentiation, suggesting that Ii-SnCs express genes important for the promotion of tissue repair but potentially detrimental immune profiles.

Ii-SnCs also expressed genes related to tissue remodeling and local tissue immune responses. Multiple cytokines, growth factors, and MMPs were differentially expressed between IR- and Ii-SnCs. GO analysis revealed differences in genes associated with bone remodeling including *Bmp*5 and *Bmp*6. Ii-SnCs increased the expression of genes such as *Il1rap*, *Tlr4*, *Cd14*, and *Csf1r* that regulate innate immune cells compared with IR-SnCs (Supplemental Table 3), providing a mechanism for T cell influence on tissue-resident innate immune cells through SnCs and the SASP. Metabolic pathways associated with insulin resistance were altered: *Il6*, *Socs3*, *Creb3l1*, and *Nfkbia* (Supplemental Table 1).

IL-4 is required for senolytic efficacy in reducing IL-17 and tissue damage after ACLT. Signatures of cellular senescence and type 17 immune responses decreased in response to i.a. senolytic treatment, but these changes did not always correlate with improved tissue integrity. Increased IL-4 expression is associated with tissue repair in muscle, cartilage, and liver (39). Expression levels of *Il4* increased 4- to 6-fold in the total joint compartment after any form of senolytic treatment in young animals compared with expression levels in controls (Figure 4A). *Il4* expression in aged animals increased 7-fold in the joint compartment only after combined i.a. plus i.p. senolysis (Figure 4A).

Systemic senolytic treatment increased LN gene expression of *Il4* in aged mice compared with expression in vehicle controls (Figure 4B), but not at the protein level (Supplemental Figure 15). We observed the opposite effect in young mice, in which the number and percentage of IL-4–expressing Th2 T cells in the draining LNs increased after senolysis, but there were no changes in gene expression by week 4 (Figure 4, B and C). Increases in *Il4* expression correlated with the efficacy of senolytic treatment in reducing tissue damage, suggesting that IL-4 may be critical for tissue integrity and restoration. Treatment with IL-17a NAb also increased *Il4* expression and promoted tissue repair. To determine whether IL-4 signaling was required for senolytic efficacy, we performed ACLT in the *Il4r*−/− mouse. Senolytic treatment in the *Il4r*−/− mouse did not reduce *Il17* expression in the LNs or alleviate pain, and we observed no decrease in cartilage tissue damage (Figure 4, D–G). To test whether IL-4 supplementation was sufficient to restore responsiveness to the senolytic agent in aged mice, we administered IL-4 with i.a. UBX0101 two weeks after ACLT. We found that *Col2a1* expression markedly increased with injection of IL-4 alone, whereas aggrecan expression moderately increased

(Supplemental Figure 14). We observed no synergistic effect with combined IL-4 and UBX0101 injection, suggesting that IL-4 alone was not adequate to restore the senolytic response or tissue integrity in aged animals (Supplemental Figure 16).

Discussion

Regenerative medicine strategies focus on stimulating tissue development but neglect to address factors that are inhibiting innate repair capacity. Here, we defined a type 17 immune profile in the articular joint after an injury that was associated with OA development. Local removal of SnCs reduced IL-17 and increased expression of IL-4 in young animals, which correlated with reduced OA development. Local removal of SnCs in aged animals reduced IL-17 but failed to increase IL-4 expression and reduce tissue damage. IL-4 expression and tissue integrity were rescued in aged animals treated with combined local and systemic senolysis. IL-4 was required for senolytic efficacy in reducing IL-17 expression and tissue damage. SnCs also induced Th17 skewing, creating a positive feedback that reinforced the chronic inflammation that inhibits tissue repair. Further analysis into the Th17-induced SnCs revealed a unique inflammation-induced senescence phenotype that included Wnts, tissue remodeling factors, and activation of innate immune pathways.

OA is associated with abnormal matrix production including sclerosis and osteophyte formation in bone and synovial thickening, suggesting a fibrotic nature of the disease (40). The role of IL-17 in musculoskeletal dysfunction is also supported by reports of IL-17a–mediated inflammation and tissue remodeling in tendons (41). IL-17 is implicated in pathologic matrix remodeling, including idiopathic lung fibrosis, Crohn's disease, and myocardial fibrosis (42–44). In other studies, SnCs have been identified as contributors to the pathology of these diseases, further corroborating the proposed connection between IL-17 and senescence (45–47).

Therapies that target IL-17 result in clinical improvements in psoriatic arthritis but have not been studied in patients with OA (48–50). Analysis of the draining LNs was critical to defining the Th17 response to joint injury and the immune changes after senolytic treatment. Cytokine changes in the LN correlated with OA disease and treatment outcomes at every time point studied. Age-related changes in LN immune cell populations and reduced Th17 cell numbers after senolytic treatment demonstrate the importance of evaluating LN changes in OA and the potential immunological effects of aging that affect disease outcomes. These findings also support the growing clinical evidence that OA is a systemic disease (51, 52).

Navi treatment did not appear to directly kill Th17 cells, since the overall CD4+ T cell numbers in the LNs and blood did not decrease. It is possible that removal of systemic SnCs that were promoting Th17 skewing was responsible for the observed immune changes. Similarly, the reduction of CD8+ T cells may have been due to direct killing by Navi or by removal of cells that induced their development. Navi is a specific inhibitor of antiapoptotic Bcl-2 family proteins (Bcl-2, Bcl-xL, and Bcl-w) and has several hematologic effects. Thrombocytopenia had a dose-limiting effect in clinical trials, though neutropenia and a reduction in circulating lymphocytes were also observed (53), consistent with the role of these pathways in lymphocyte maturation (54). As a comparison

with the aged animals, we used 10-week-old mice for young controls. This age allows immunological analysis in which there is less of an impact of environmental factors, which can skew immune cell phenotypes (55, 56). However, mice are not considered fully skeletally mature until 12 weeks of age, so the joint injury, tissue quality, and resulting cellular changes may be affected (57, 58).

Th17 cells provide a defense against extracellular pathogens and fungal immunity, but pathogenic Th17 tissue responses are involved in autoimmunity including inflammatory arthritis (59). Increased levels of IL-17a and IL-23 have been identified in patients with OA, however, little research has been conducted to further elucidate how the IL-17/IL-23 axis affects disease (17, 60). IL-23 stabilizes and supports the generation of pathogenic Th17 cells (61, 62). IL-23 is produced by activated macrophages but has no effect on naive T cells. T cells only express the IL-23 receptor after activation with IL-6 (63–65). IL-23p19–deficient mice, which do not have IL-17–producing CD4+ T cells, are protected from the formation of collagen-induced arthritis.

The capacity to clear SnCs after trauma may vary depending on the tissue type and age. SnCs secrete cytokines that may be responsible in part for the induction of a type 17 immune response after joint trauma, and, likewise, Th17 cells may be responsible for senescence induction. The articular joint with its thick extracellular matrix and limited vascular access may be especially challenging for both SnC clearance and resolution of inflammation, leading to the Th17 senescence positive reinforcement that promotes chronic inflammation and inhibits tissue repair. Further affecting tissue integrity, the number of immune cells and stem cells decreases with age, whereas overall cytokine expression levels remain high. Furthermore, we were also able to reduce tissue damage in aged animals after local and systemic senolysis, suggesting that reduced stem cell numbers may not be a limiting factor. The challenge with tissue repair in older animals may be due instead to the accumulation of SnCs throughout the body that induce increased local and systemic Th17 skewing. Furthermore, impaired immune activity in aged animals may also reduce SnC clearance (66). Systemic SnC clearance recovers bone marrow myeloid skewing that occurs with aging and may also restore T cell numbers to modulate the balance of effector T cells and promote stem cell function (33). There is still a lack of understanding of the phenotype of senescent cells in vivo, how they differ between tissues, and mechanisms for how senolytics may selectively clear these cells. In the present study, it was not clear why UBX0101 cleared SnCs in the joint but Navi did not, despite its ability to clear SnCs in multiple other tissue types. Future studies will aim to delineate these mechanisms.

The SASP, composed of proinflammatory cytokines, is central to the pathology of SnCs, and the distinct SASP produced by Th17 cells introduces previously unrecognized mechanisms of tissue pathology and molecular targets to inhibit or reverse senescence. SASP activation of innate and adaptive immune cells may amplify the effect of SnCs, which are usually small in number. It also introduces a potential mechanism for local SnCs to exert systemic effects. The SASP factors IL-6 and IL-1β promote T cell skewing toward a type 17 immune profile when TGF-β is also present, further amplifying the T cell response (35). In the case of the articular joint, TGF-β is produced in the subchondral bone, and blocking its activity in bone reduces OA progression (32). Ultimately, tissue-specific production of TGF-β may impact the Th17/senescence axis to modulate inflammation and tissue pathology.

The positive feedback between SnCs and the type 17 immune response reinforces the chronic inflammation that actively blocks tissue repair. Th17 differentiation requires the transcription factor STAT3, which negatively regulates IL-4 production (67). IL-4 is integral for healing in multiple tissues and was central to achieving healing after SnC and IL-17 reduction in the joint (39, 68). STAT3 also negatively affects the regulatory CD4+ T cell subset (Tregs) that suppresses inflammation and promotes tolerance to self-antigens and tissue homeostasis (69). On the other hand, STAT3 serves as an important promoter of tissue development. LIF and Wnts converge to promote a STAT3-related stem cell function that is relevant to embryological development and tissue repair in several tissues including cartilage. T cells are not present during STAT3-relevant tissue formation in embryological development, but the presence of T cells during STAT3 activation in the injury response designed to support tissue repair may also lead to detrimental Th17 activation and chronic inflammation. Thus, the kinetics of the immune response after injury and delayed immune cell clearance may create an environment with conflicting effects of STAT3 activation.

Neutralization of IL-17a in the articular joint reduced Cdkn1a, but not Cdkn2a, expression. Diekman et al. found that p16INK4a is a marker of chondrocyte aging but does not itself cause OA (70). In other studies, they found that knockdown of the cell-cycle inhibitor p21 enhanced cartilage formation (71). Since the decrease in Cdkn1a expression paralleled the decrease in tissue inflammation and increased cartilage formation, IL-17 neutralization may reduce the SASP and many features of senescence, but there remains discordance with Cdkn2a expression. The immunological and SASP connection may differ between p16 INK4a and p21, and further studies may further elucidate the cell-cycle properties of trauma- and age-induced senescent cells.

Despite the reduced regenerative capacity associated with aging, we were able to reduce OA development after injury in aged animals, without the addition of exogenous stem cells or growth factors. In tissue repair in the articular joint, activation of the Th17/senescence axis may be a critical factor that is also relevant in other nonhealing wounds. The systemic T cell changes after senolysis suggest that CD8+ T cells and Th17 cells may be key factors inhibiting tissue repair in an aged environment characterized by an increased senescence burden and inflammation. This is supported by studies showing that differentiated CD8+ T cells negatively regulate bone repair (72). Systemic and environmental factors beyond aging that increase IL-17 may also influence the development of chronic inflammation and reduce tissue repair capacity. The discovery of Th17 induction of senescence represents a physiologically relevant class of SnCs. The unique SASP of the immunologically induced SnCs introduces mechanisms for the role of senescence in tissue development, tissue repair, and immune modulation.

Methods

Surgical procedures. OA was induced by ACLT (73) in 10-week-old or 72-week-old male C57BL/6 mice and 10-week-old *Il4r−/−* mice from Charles River Laboratories. For senolytic treatments, 6 doses of 10

μL injections of either vehicle control (5% DMSO and 95% PBS) or UBX0101 were administered into the joint of the operated knee via a 30-gauge needle or i.p. The joint cavity was opened in the sham group, but the ACL was not transected. For IL-17a neutralization experiments, IL-17a antibody (Mouse IgG1 kappa Isotype, Amgen) or an isotype control antibody (Mouse IgG1 kappa Isotype, catalog 16-4714-81, BioLegend) was administered every other day, starting 1 week after ACLT, for 5 total doses delivered either i.a. (5 μg/dose) or i.p. (100 μg/dose). For IL-4 supplementation experiments, 72-week-old C57BL/6 mice were obtained from The Jackson Laboratory, and 6 doses of IL-4 complex (catalog 214-14, PeproTech; 2 μg in 10 μL), UBX0101 (10 μL of 1 mM), or a combination of both were administered into the joint space 2 weeks after ACLT surgery. IL-4 supplementation was delivered in the form of a half-life–stabilized IL-4–anti–IL-4 mAb complex (Il-4c).

Nonsurgical animal experiments. Navi was delivered i.p. for 5 consecutive days (50 mg/kg/d). Blood was drawn before or 1 or 2 weeks after injection, and inguinal LNs were harvested 2 weeks after Navi treatment and their cells analyzed by flow cytometry. The panel used the following antibodies: Viability Dye eFlour 780 (catalog 65-0865-14, eBioscience), CD45 in BV605 (catalog 109841, BioLegend), CD3 in phycoerythrin (PE) (catalog 100307, BioLegend), CD19 in PerCP-Cy5.5 (catalog 115533, BioLegend), CD4 in FITC (catalog 100405, BioLegend), and CD8a in BV711 (catalog 100747, BioLegend).

Histological evaluation. After 4 weeks, mouse knees were fixed in 4% paraformaldehyde, decalcified for 2 weeks in 10% EDTA, and then dehydrated and embedded in paraffin. Sections (7 μm thick) were taken and stained with Safranin-O and Fast Green (Applied Biosciences) according to the manufacturer's instructions. OARSI scores are based on blinded histological assessment of the medial plateau of the tibia (74). Osteophytes on the tibial plateau were scored from 0 to 3, with 0 indicating no osteophytes or an osteophyte up to 100 μm in diameter; a score of 1 indicating an osteophyte measuring 100–200 μm in diameter; a score of 2 indicating an osteophyte of 200–300 μm in diameter; and a score of 3 indicating an osteophyte measuring more than 300 μm in diameter (75).

Quantification of subchondral bone damage. Osteophyte thickness was measured with AxioVision SE64 software. Medial tibial bone sclerosis was scored by measuring the subchondral trabecular bone to marrow ratio. On each safranin O–stained joint section, the decrease or increase in trabecular bone area was assigned a score from −5 to 5: a score of 0 represents no increase or decrease, −5 represents severe bone loss, and 5 represents severe bone sclerosis.

Immunofluorescence. Slides were deparaffinized and antigen retrieval performed in boiling citrate antigen retrieval buffer (ARB) for 20 minutes. Slides were blocked in 1.5% BSA, 1.5% normal goat serum, and 0.05% Tween 20 for 45 minutes before application of primary antibodies. Staining for IL-17 was done using rabbit anti–IL-17 antibody (ab79056, Abcam) at a 1:400 dilution. Rat anti-CD4 (clone 4SM95, eBioscience) was used at a 1:200 dilution. Secondary antibodies were applied at room temperature for 2 hours (anti–rat AF488 catalog A-11006; anti–rabbit AF594, catalog A-11037, Thermo Fisher Scientific) and followed by DAPI staining for 5 minutes before mounting.

Gene expression analysis. Mouse joints were frozen in liquid nitrogen and homogenized using a sterile mortar and pestle. Inguinal LNs were crushed in a 1.5 mL Biomasher tube (Kimble). RNA was extracted using TRIzol Reagent (Life Technologies, Thermo Fisher Scientific) following the manufacturer's protocol. cDNA was synthesized using Superscript III Reverse Transcriptase (Life Technologies, Thermo Fisher Scientif-

ic) following the manufacturer's protocol. Quantitative real-time PCR (qRT-PCR) was carried out using SYBR Green primers and a StepOne-Plus Real-time PCR System (Life Technologies, Thermo Fisher Scientific). Relative gene expression was calculated by the $\Delta\Delta$Ct method. The ΔCt was calculated using the reference genes β2-microglobulin (*B2m*) and β-actin (*Actb*). The $\Delta\Delta$Ct was calculated relative to the unoperated control group. The following mouse-specific primers were used: *Actb* forward, CCACCGTGAAAAGATGACCC, *Actb* reverse, GTAGATGG-GCACAGTGTGGG; *B2m* forward, CTCGGTGACCCTGGTCTTTC, *B2m* reverse, GGATTTCAATGTGAGGCGGG; *Acan* forward, CGTTG-CAGACCAGGAGCAAT, *Acan* reverse, CGGTCATGAAAGTGGCGG-TA; *Col2a1* forward, CCTCCGTCTACTGTCCACTGA, *Col2a1* reverse, ATTGGAGCCCTGGATGAGCA; *Mmp13* forward, GTCTTCATCG-CCTGGACCATA, *Mmp13* reverse, GGAGCCCTGATGTTTCCCAT; *Runx2* forward, GCCGGGAATGATGAGAACTA, *Runx2* reverse, GGTGAAACTCTTGCCTCGTC; *Il4* forward, ACAGGAGAAGGGAC-GCCAT, *Il4* reverse, ACCTTGGAAGCCCTACAGA; *Il10* forward, TCTCACCCAGGGAATTCAAA, *Il10* reverse, AAGTGATGCCCCAG-GCA; *Il6* forward, CCAGGTAGCTATGGTACTCCAGAA, *Il6* reverse, GCTACCAAACTGGATATAATCAGGA; and *IL1b* forward, GTATGG-GCTGGACTGTTTC, *IL1b* reverse, GCTGTCTGCTCATTCACG. *Il17* expression in LNs was assessed using the following SYBR Green primer: *Il17a* forward, TCAGCGTGTCCAAACACTGAG, *Il17a* reverse, CGC-CAAGGGAGTTAAAGACTT.

TaqMan primers were used for detection of *Il17f* and *Il23a* in joint tissues. The IDs are as follows: *Il23a*, Mm00518984_m1; *Il17a*, Mm00439618_m1; *Il17f*, Mm00521423_m1; *B2m*, Mm00437762_m1; and *Actb*, Mm04394036_g1.

Preamplification. Preamplification was performed on cDNA before gene expression analysis using TaqMan PreAmp Master Mix (Thermo Fisher Scientific). *Il17f*, *Il23a*, *Gm-Csf* (*Csf2*), and *Ptgs2* were preamplified for 10 cycles.

Flow cytometry. Whole joints and inguinal LNs were harvested 1, 2, and 4 weeks after surgery. Blood was collected in EDTA-coated tubes and treated with ammonium chloride potassium (ACK) lysing buffer (Thermo Fisher Scientific). Joint tissue was diced and digested for 45 minutes at 37°C in 1.67 Wünsch U/mL Liberase TL (Roche Diagnostics) plus 0.2 mg/mL DNase I (Roche Diagnostics) in serum-free RPMI-1640 Medium (Gibco, Thermo Fisher Scientific) on a shaker at 400 rpm. The digest was filtered through a 70 μm cell strainer (Thermo Fisher Scientific) and then washed with 1× PBS.

The T cell panel displayed in Figure 1 included the following: Fixable Viability Dye eFluor 780 (catalog 65-0865-14, eBioscience), CD45 V500 (catalog 561487, BD biosciences), CD3 Alexa Fluor 488 (catalog 100212, BioLegend), CD4 PE-Cy7 (catalog 100421, BioLegend), CD8 BV711 (catalog 100747, BioLegend), NK1.1 BV605 (catalog 108739, BioLegend), Thy1.2 Pacific Blue (catalog 140305, BioLegend), γδ TCR PE-CF594 (catalog 563532, BD Biosciences), IL-4 PerCP-Cy5.5 (catalog 504123, BioLegend), IFN-γ APC (catalog 505809, BioLegend), IL-17a AF700 (catalog 506914, BioLegend), and IL-17f PE (catalog 12-7471-82, eBioscience). Cytokine staining followed fixation and permeabilization with a BD CytoFix/CytoPerm Kit (BD Biosciences). Analyses were performed using FlowJo Flow Cytometry Analysis Software (Tree Star).

FACS. ILCs from joints were sorted 2 weeks after ACLT. Tissue processing and antibody information is the same as described above. Dead cells were excluded using Fixable Viability Dye eFluor 780

(Thermo Fisher Scientific), and only surface staining was performed to keep the cells alive during staining for CD45, CD3, CD4, CD8, and Thy1.2. Cells were sorted on a BD FACSAria Fusion SORP for live, CD45^{+}, CD3^{–}, CD4^{–}, CD8^{–}, and Thy1.2^{+} cells identified as ILCs.

Hind limb weight-bearing assessment. Weight bearing by mice was measured using an incapacitance tester (Columbus Instruments). The percentage of weight distributed on the ACLT limb was used as an index of joint discomfort in OA (73). The mice were positioned to stand on their hind paws in an angled box placed above the incapacitance tester so that each hind paw rested on a separate force plate. The force (*g*) exerted by each limb was measured. Three consecutive 3-second readings were taken and averaged to obtain the mean score (76).

Hind limb responsiveness. Mice were placed on the hotplate at 55°C. The latency period for hind limb response (jumping or paw licking) was recorded as the response time before surgery and 2 and 4 weeks after surgery in all animal groups (73). Three readings were taken per mouse and averaged to obtain the mean response time.

Murine cell culture and coculture conditions. NIH 3T3 fibroblasts (MilliporeSigma) were cultured for 7 days in fibroblast culture medium. The cells were then irradiated with CIXD Biological Irradiator 10 Gy (Xstrahl) and collected after 7 days. When SnCs were harvested, naive CD4^{+} T cells were isolated from the LNs of 6-week-old C57BL/6 mice. The Naive CD4^{+} T cell Isolation Kit and MACS Column from Miltenyi Biotec were used according to the manufacturer's instructions. T cell purity was assessed by flow cytometry using the following panel: Fixable Viability Dye Aqua (catalog L34957, Thermo Fisher Scientific); CD45 V500, CD3 Alexa Fluor 488, CD4 PE-Cy7, CD8 BV711, CD44 BV605 (catalog 103047, BioLegend); and CD62L APC-CY7 (catalog 104411, BioLegend; CD45, CD3, CD4, and CD8 antibody information is provided above). We found that 92.9% of the CD4^{+} T cell population was naive. T cells and SnCs were seeded in 12-well Transwell plates at 500,000 and 300,000 cells/per well, respectively. T cells were cultured with an equal number of magnetic beads from the Dynabeads Mouse T-activator CD3/CD28 Kit (Thermo Fisher Scientific). IMDM medium supplemented with 10% FBS, 5% penicillin/streptomycin, and 1% sodium pyruvate was used. The "SnC" group consisted of T cells plus SnCs; the "SnC + IL-2" group had the addition of 500 unit/mL IL-2 into the culture medium; the "SnC + IL-2 + TGF-β" group also had the addition of 2 ng/mL Recombinant Human TGF-β (PeproTech); the "TGF-β" group consisted of IL-2 plus TGF-β. The control groups consisted of naive T cells plus IL-2 and T cells skewed to Th17 using a Th17 Cell Differentiation K (R&D Systems). After 3 days in culture, 50% of the media was aliquoted, and fresh media were added. After 5 total days in coculture, T cells were harvested for flow cytometric and qRT-PCR analysis. T cells were stained for Fixable Viability Dye eFluor 780, CD45 V500, CD3 Alexa Fluor 488, CD4 PE-Cy7, CD8 BV711, IL4 PerCP-Cy5.5, IFN-γ APC, IL-17a AF700, and IL-17f PE (all antibody information is provided above). IL-4, IL-17a, IL-17f, and IFN-γ staining followed fixation and permeabilization with a BD Cytofix/Cytoperm Kit (BD Biosciences).

Th17 T cells cocultured with healthy fibroblasts. Naive CD4^{+} T cells were isolated as described above and Th17 skewed using the CellXVivo Mouse Th17 Differentiation Kit (R&D Systems) for 4 days before coculture with healthy fibroblasts. Seven days after the start of the T cell culture (day 3 of the coculture), T cells were restimulated with fresh CD3^{+}CD28^{+} Dynabeads. Healthy fibroblasts and Th17 cells were cocultured in a 12-well Transwell plate (3 μm

pore size membranes), with 500,000 fibroblasts and 500,000 Th17 cells per well. Cells were harvested 3 and 7 days after the start of the coculture, at which time fibroblasts were harvested for qRT-PCR and stained with SA–β-gal.

NanoString gene expression analysis. Normal murine fibroblasts cocultured with Th17 cells or after irradiation were used to isolate mRNA for NanoString analysis (NanoString Technologies). Gene expression was evaluated using the NanoString Cancer Pathway Panel (XT-CSO-MIP1-12). RNA (100 μg) was added to a barcoded probe set mixture and hybridized for 20 hours at 65°C. All hybridized samples were processed using a NanoString Prep Station operating under high-sensitivity mode, and mRNA target transcripts were counted using the NanoString nCounter Digital Analyzer System. Data were analyzed using NanoString nSolver software, version 3.0. The top-50 differentially regulated genes were uploaded into the Database for Annotation, Visualization, and Integrated Discovery (DAVID) functional annotation tool (https://david.ncifcrf.gov/), and GO was run to calculate significantly enriched gene sets.

SA–β-gal staining. SA–β-gal staining was performed as previously described (1). A SA–β-gal Staining Kit (K320-250, BioVision) was used according to the manufacturer's instructions. SnCs were identified as blue-stained cells under light microscopy. Total cells were counted using a nuclear DAPI counterstain in 10 random fields per culture dish to determine the percentage of SA–β-gal^{+} cells.

Human cell coculture. Human OA cartilage (National Disease Research Interchange [NDRI]) was diced and digested for 16 hours to isolate chondrocytes. Chondrocytes were plated for 2 days, followed by sorting on a BD FACSAria IIu Cell Sorter on the basis of size. Human T cells were harvested from peripheral blood via Ficoll-Paque (MilliporeSigma) density separation, followed by CD4^{+} T cell selection using the Miltenyi Biotec Human CD4^{+} T cell Isolation Kit and a MACS column. The purity of CD4^{+} T cells was assessed by flow cytometry using the following panel: Fixable Viability Dye Aqua; CD45 BV605 (catalog 368523, BioLegend); CD3 Alexa Fluor 700 (catalog 300323, BioLegend); CD4 PE-Cy7 (catalog 357410, BioLegend); and CD8 APC-Cy7 (catalog 344713, BioLegend). We found that 95% of CD3^{+} T cells were CD4^{+}CD8^{–}. T cells and Snc chondrocytes were seeded into a 12-well Transwell plate at approximately 400,000 and approximately 150,000 cells per well, respectively. T cells were cultured with an equal number of magnetic beads using the Dynabeads Human T-activator CD3/CD28 Kit (Thermo Fisher Scientific). Cells were cocultured for 5- and 7-day endpoints to assess cytokine activity. Media with TGF-β were supplemented with 2 ng/mL Recombinant Human TGF-β. The culture media consisted of 50% AIM V media and 50% IMDM, 5% FBS, 1% penicillin/streptomycin, 1% nonessential amino acids (NEAA), and 1% NaPyrv (all from Gibco, Thermo Fisher Scientific). Media were supplemented as needed, and on day 3, one-third of the media was removed and replaced with fresh media. The Th17 control condition was made using the CellXVivo Human Th17 Differentiation Kit (R&D Systems).

T cells were stained for Fixable Viability Dye Aqua, CD45, CD3, CD4, CD8 (antibody information is provided above), IL-4 PE (catalog 500703, BioLegend), IFN-γ APC (catalog 502511, BioLegend), FoxP3 AF488 (catalog 320111, BioLegend), IL-17a BV421 (catalog 512322, BioLegend), and IL-17f PE-CF594 (catalog 564263, BD Biosciences). Cytokine staining followed fixation and permeabilization with the BD Cytofix/Cytoperm Kit (BD Biosciences).

Statistics. Statistical analysis was performed using a 1-way ANOVA with Holm-Šidák multiple-comparisons correction in GraphPad Prism (GraphPad Software). For in vivo and in vitro experiments, all groups were compared with each other unless otherwise noted here or in the figure legends. In Figure 1, E–G, separate 1-way ANOVAs were performed for each time point. For senolytic experiments, separate 1-way ANOVAs were performed for young and aged groups, and the experimental groups were compared with the control group (vehicle). For the in vitro experiment in Figure 3B, a 2-tailed Student's *t* test was performed within each time point. A *P* values of less than 0.05 was considered significant.

Study approval. All animal procedures were approved by the IACUC of Johns Hopkins University. Human OA cartilage was obtained from postmortem tissue from the NDRI under a protocol approved by the IRB of Johns Hopkins University (IRB00088842).

Author contributions

HJF, HZ, and JHE conceived the studies, designed experiments, and wrote the manuscript. HJF and HZ analyzed data. JH contributed to IL-17 neutralization studies and Navi experiments in noninjured mice. JHE, OHJ, KS, COB, FH, DMP, DZ, JC, and MTW contributed to experimental design and interpretation of the results. ANP, LC, DRM, and AJT provided guidance for in vitro studies. DRM contributed to qRT-PCR work in Supplemental Figure 6. All authors participated in editing and revising the manuscript text and figures. HJF performed joint and LN immune cell profiling and qRT-PCR characterization, ILC sorting, and NanoString analysis. HJF and MTW performed and analyzed flow cytometric data on cells from the aged animals. HJF performed immunofluorescence staining for F4/80, CD11b, IL-17, and IL-23, analyzed qRT-PCR results from aged and young joint and LN tissue, and performed IL-17a neutralization experiments and analysis. HZ performed surgeries on aged mice, immunofluorescence p16 staining, senolytic experiments in young and aged animals and analysis, T cell coculture experiments, NanoString experiments, and *Il4r−/−* and IL-4 neutralization experiments and analysis. HZ and MTW performed flow cytometry experiments and analysis of cells from aged and young animals that underwent senolytic treatment and ACLT. HJF and HZ performed in vitro human T cell culture and analysis.

Acknowledgments

Address correspondence to: Jennifer H. Elisseeff, Department of Biomedical Engineering, Johns Hopkins University School of Medicine, Smith Building 5031, 400 N. Broadway, Baltimore, Maryland 21231, USA. Email: jhe@jhu.edu.

1. Jeon OH, et al. Local clearance of senescent cells attenuates the development of post-traumatic osteoarthritis and creates a pro-regenerative environment. *Nat Med*. 2017;23(6):775–781.

2. Blau HM, Cosgrove BD, Ho AT. The central role of muscle stem cells in regenerative failure with aging. *Nat Med*. 2015;21(8):854–862.

3. Bussian TJ, Aziz A, Meyer CF, Swenson BL, van Deursen JM, Baker DJ. Clearance of senescent glial cells prevents tau-dependent pathology and cognitive decline. *Nature*. 2018;562(7728):578–582.

4. Childs BG, Baker DJ, Wijshake T, Conover CA, Campisi J, van Deursen JM. Senescent intimal foam cells are deleterious at all stages of atherosclerosis. *Science*. 2016;354(6311):472–477.

5. Demaria M, et al. An essential role for senescent cells in optimal wound healing through secretion of PDGF-AA. *Dev Cell*. 2014;31(6):722–733.

6. Coppé JP, Desprez PY, Krtolica A, Campisi J. The senescence-associated secretory phenotype: the dark side of tumor suppression. *Annu Rev Pathol*. 2010;5:99–118.

7. Vicente R, Mausset-Bonnefont AL, Jorgensen C, Louis-Plence P, Brondello JM. Cellular senescence impact on immune cell fate and function. *Aging Cell*. 2016;15(3):400–406.

8. Xu M, et al. Transplanted senescent cells induce an osteoarthritis-like condition in mice. *J Gerontol A Biol Sci Med Sci*. 2017;72(6):780–785.

9. Howcroft TK, et al. The role of inflammation in age-related disease. *Aging (Albany NY)*. 2013;5(1):84–93.

10. Campisi J, Robert L. Cell senescence: role in aging and age-related diseases. *Interdiscip Top Gerontol*. 2014;39:45–61.

11. Montecino-Rodriguez E, Berent-Maoz B, Dorshkind K. Causes, consequences, and reversal of immune system aging. *J Clin Invest*. 2013;123(3):958–965.

12. Sanada F, et al. Source of chronic inflammation in aging. *Front Cardiovasc Med*. 2018;5:12.

13. Frasca D, Blomberg BB. Inflammaging decreases adaptive and innate immune responses in mice and humans. *Biogerontology*. 2016;17(1):7–19.

14. Schmitt V, Rink L, Uciechowski P. The Th17/Treg balance is disturbed during aging. *Exp Gerontol*. 2013;48(12):1379–1386.

15. Jeon OH, David N, Campisi J, Elisseeff JH. Senescent cells and osteoarthritis: a painful connection. *J Clin Invest*. 2018;128(4):1229–1237.

16. Lurati A, Laria A, Gatti A, Brando B, Scarpellini M. Different T cells' distribution and activation degree of Th17 CD4+ cells in peripheral blood in patients with osteoarthritis, rheumatoid arthritis, and healthy donors: preliminary results of the MAGENTA CLICAO study. *Open Access Rheumatol*. 2015;7:63–68.

17. Askari A, et al. Increased serum levels of IL-17A and IL-23 are associated with decreased vitamin D3 and increased pain in osteoarthritis. *PLoS ONE*. 2016;11(11):e0164757.

18. Ishii H, Tanaka H, Katoh K, Nakamura H, Nagashima M, Yoshino S. Characterization of infiltrating T cells and Th1/Th2-type cytokines in the synovium of patients with osteoarthritis. *Osteoarthr Cartil*. 2002;10(4):277–281.

19. Raychaudhuri SP, Raychaudhuri SK. Mechanistic rationales for targeting interleukin-17A in spondyloarthritis. *Arthritis Res Ther*. 2017;19(1):51.

20. Lubrano E, Perrotta FM. Secukinumab for ankylosing spondylitis and psoriatic arthritis. *Ther Clin Risk Manag*. 2016;12:1587–1592.

21. Robinson WH, et al. Low-grade inflammation as a key mediator of the pathogenesis of osteoarthritis. *Nat Rev Rheumatol*. 2016;12(10):580–592.

22. Jotanovic Z, Mihelic R, Sestan B, Dembic Z. Role of interleukin-1 inhibitors in osteoarthritis: an evidence-based review. *Drugs Aging*. 2012;29(5):343–358.

23. Calich AL, Domiciano DS, Fuller R. Osteoarthritis: can anti-cytokine therapy play a role in treatment? *Clin Rheumatol*. 2010;29(5):451–455.

24. Cai J, Weiss ML, Rao MS. In search of "stemness". *Exp Hematol*. 2004;32(7):585–598.

25. Gaffen SL, Jain R, Garg AV, Cua DJ. The IL-23-IL-17 immune axis: from mechanisms to therapeutic testing. *Nat Rev Immunol*. 2014;14(9):585–600.

26. Binks DA, et al. Role of vascular channels as a novel mechanism for subchondral bone damage at cruciate ligament entheses in osteoarthritis and inflammatory arthritis. *Ann Rheum Dis*. 2015;74(1):196–203.

27. Elemam NM, Hannawi S, Maghazachi AA. Innate lymphoid cells (ILCs) as mediators of inflammation, release of cytokines and lytic molecules. *Toxins (Basel)*. 2017;9(12):E398.

28. Symowski C, Voehringer D. Interactions between innate lymphoid cells and cells of the innate and adaptive immune system. *Front Immunol*. 2017;8:1422.

29. Robinette ML, et al. Transcriptional programs define molecular characteristics of innate lymphoid cell classes and subsets. *Nat Immunol*. 2015;16(3):306–317.

30. Koh TJ, DiPietro LA. Inflammation and wound healing: the role of the macrophage. *Expert Rev*

Mol Med. 2011;13:e23.

31. Childs BG, Durik M, Baker DJ, van Deursen JM. Cellular senescence in aging and age-related disease: from mechanisms to therapy. *Nat Med*. 2015;21(12):1424–1435.

32. Zhen G, et al. Inhibition of TGF-β signaling in mesenchymal stem cells of subchondral bone attenuates osteoarthritis. *Nat Med*. 2013;19(6):704–712.

33. Chang J, et al. Clearance of senescent cells by ABT263 rejuvenates aged hematopoietic stem cells in mice. *Nat Med*. 2016;22(1):78–83.

34. Dimri GP, et al. A biomarker that identifies senescent human cells in culture and in aging skin in vivo. *Proc Natl Acad Sci USA*. 1995;92(20):9363–9367.

35. Korn T, Bettelli E, Oukka M, Kuchroo VK. IL-17 and Th17 cells. *Annu Rev Immunol*. 2009;27:485–517.

36. Yang Y, Topol L, Lee H, Wu J. Wnt5a and Wnt5b exhibit distinct activities in coordinating chondrocyte proliferation and differentiation. *Development*. 2003;130(5):1003–1015.

37. Onishi K, Zandstra PW. LIF signaling in stem cells and development. *Development*. 2015;142(13):2230–2236.

38. Metcalfe SM. LIF in the regulation of T-cell fate and as a potential therapeutic. *Genes Immun*. 2011;12(3):157–168.

39. Sadtler K, et al. Developing a pro-regenerative biomaterial scaffold microenvironment requires T helper 2 cells. *Science*. 2016;352(6283):366–370.

40. Mathiessen A, Conaghan PG. Synovitis in osteoarthritis: current understanding with therapeutic implications. *Arthritis Res Ther*. 2017;19(1):18.

41. Millar NL, et al. IL-17A mediates inflammatory and tissue remodelling events in early human tendinopathy. *Sci Rep*. 2016;6:27149.

42. Mi S, et al. Blocking IL-17A promotes the resolution of pulmonary inflammation and fibrosis via TGF-beta1-dependent and -independent mechanisms. *J Immunol*. 2011;187(6):3003–3014.

43. Siakavellas SI, Bamias G. Role of the IL-23/IL-17 axis in Crohn's disease. *Discov Med*. 2012;14(77):253–262.

44. Liu Y, et al. IL-17 contributes to cardiac fibrosis following experimental autoimmune myocarditis by a PKCβ/Erk1/2/NF-κB-dependent signaling pathway. *Int Immunol*. 2012;24(10):605–612.

45. Waters DW, et al. Fibroblast senescence in the pathology of idiopathic pulmonary fibrosis. *Am J Physiol Lung Cell Mol Physiol*. 2018;315(2):L162–L172.

46. Sohn JJ, et al. Macrophages, nitric oxide and microRNAs are associated with DNA damage response pathway and senescence in inflammatory bowel disease. *PLoS ONE*. 2012;7(9):e44156.

47. Biernacka A, Frangogiannis NG. Aging and cardiac fibrosis. *Aging Dis*. 2011;2(2):158–173.

48. Mease PJ. Inhibition of interleukin-17, interleukin-23 and the TH17 cell pathway in the treatment of psoriatic arthritis and psoriasis. *Curr Opin Rheumatol*. 2015;27(2):127–133.

49. Raychaudhuri SK, Saxena A, Raychaudhuri SP. Role of IL-17 in the pathogenesis of psoriatic arthritis and axial spondyloarthritis. *Clin Rheumatol*. 2015;34(6):1019–1023.

50. Raychaudhuri SP, Raychaudhuri SK. IL-23/IL-17 axis in spondyloarthritis-bench to bedside. *Clin Rheumatol*. 2016;35(6):1437–1441.

51. Perruccio AV, Chandran V, Power JD, Kapoor M, Mahomed NN, Gandhi R. Systemic inflammation and painful joint burden in osteoarthritis: a matter of sex? *Osteoarthr Cartil*. 2017;25(1):53–59.

52. Haugen IK. The puzzle of generalized osteoarthritis (OA) -- is OA a systemic enthesopathy? *J Rheumatol*. 2012;39(2):203–205.

53. Wilson WH, et al. Navitoclax, a targeted high-affinity inhibitor of BCL-2, in lymphoid malignancies: a phase 1 dose-escalation study of safety, pharmacokinetics, pharmacodynamics, and antitumour activity. *Lancet Oncol*. 2010;11(12):1149–1159.

54. Cory S. Regulation of lymphocyte survival by the bcl-2 gene family. *Annu Rev Immunol*. 1995;13:513–543.

55. Busse PJ, Mathur SK. Age-related changes in immune function: effect on airway inflammation. *J Allergy Clin Immunol*. 2010;126(4):690–699.

56. Tao L, Reese TA. Making mouse models that reflect human immune responses. *Trends Immunol*. 2017;38(3):181–193.

57. Ferguson VL, Ayers RA, Bateman TA, Simske SJ. Bone development and age-related bone loss in male C57BL/6J mice. *Bone*. 2003;33(3):387–398.

58. Fang H, Beier F. Mouse models of osteoarthritis: modelling risk factors and assessing outcomes. *Nat Rev Rheumatol*. 2014;10(7):413–421.

59. Lee Y, Kuchroo V. Defining the functional states of Th17 cells. *F1000Res*. 2015;4(F1000 Faculty Rev):132.

60. Chen B, Deng Y, Tan Y, Qin J, Chen LB. Association between severity of knee osteoarthritis and serum and synovial fluid interleukin 17 concentrations. *J Int Med Res*. 2014;42(1):138–144.

61. Lubberts E. The IL-23-IL-17 axis in inflammatory arthritis. *Nat Rev Rheumatol*. 2015;11(10):562.

62. Murphy CA, et al. Divergent pro- and anti-inflammatory roles for IL-23 and IL-12 in joint autoimmune inflammation. *J Exp Med*. 2003;198(12):1951–1957.

63. Croxford AL, Mair F, Becher B. IL-23: one cytokine in control of autoimmunity. *Eur J Immunol*. 2012;42(9):2263–2273.

64. Oppmann B, et al. Novel p19 protein engages IL-12p40 to form a cytokine, IL-23, with biological activities similar as well as distinct from IL-12. *Immunity*. 2000;13(5):715–725.

65. Lyakh L, Trinchieri G, Provezza L, Carra G, Gerosa F. Regulation of interleukin-12/interleukin-23 production and the T-helper 17 response in humans. *Immunol Rev*. 2008;226:112–131.

66. Ovadya Y, et al. Impaired immune surveillance accelerates accumulation of senescent cells and aging. *Nat Commun*. 2018;9(1):5435.

67. August A. Who regulates whom: ZNF341 is an additional player in the STAT3/T$_H$17 song. *Sci Immunol*. 2018;3(24):eaat9779.

68. Heredia JE, et al. Type 2 innate signals stimulate fibro/adipogenic progenitors to facilitate muscle regeneration. *Cell*. 2013;153(2):376–388.

69. Corthay A. How do regulatory T cells work? *Scand J Immunol*. 2009;70(4):326–336.

70. Diekman BO, et al. Expression of p16[INK4a] is a biomarker of chondrocyte aging but does not cause osteoarthritis. *Aging Cell*. 2018;17(4):e12771.

71. Diekman BO, et al. Knockdown of the cell cycle inhibitor p21 enhances cartilage formation by induced pluripotent stem cells. *Tissue Eng Part A*. 2015;21(7-8):1261–1274.

72. Reinke S, et al. Terminally differentiated CD8^{+} T cells negatively affect bone regeneration in humans. *Sci Transl Med*. 2013;5(177):177ra36.

73. Ruan MZ, Patel RM, Dawson BC, Jiang MM, Lee BH. Pain, motor and gait assessment of murine osteoarthritis in a cruciate ligament transection model. *Osteoarthr Cartil*. 2013;21(9):1355–1364.

74. Glasson SS, Chambers MG, Van Den Berg WB, Little CB. The OARSI histopathology initiative - recommendations for histological assessments of osteoarthritis in the mouse. *Osteoarthr Cartil*. 2010;18 Suppl 3:S17–S23.

75. Miller RE, et al. CCR2 chemokine receptor signaling mediates pain in experimental osteoarthritis. *Proc Natl Acad Sci USA*. 2012;109(50):20602–20607.

76. Ruan MZ, et al. Proteoglycan 4 expression protects against the development of osteoarthritis. *Sci Transl Med*. 2013;5(176):176ra34.